Computer simulation of the 60° dislocation interaction with vacancy cluster in silicon

Chengxiang Li,* Qingyuan Meng, Kangyou Zhong, and Chaoying Wang
Department of Astronautical Science and Mechanics, Harbin Institute of Technology, Harbin 150001, People's Republic of China
(Received 13 April 2007; revised manuscript received 1 October 2007; published 28 January 2008; corrected 30 January 2008)

In the current work, the interaction of the 60° shuffle dislocation with the vacancy cluster under applied shear stress in silicon crystal is studied via the molecular dynamics method. Stillinger-Weber (SW) potential and environment-dependent interatomic potential (EDIP) are used to calculate the interatomic forces. Simulation results show that at low shear stress, the dislocation is pinned by a vacancy cluster. With the stress level increased to a certain critical value σ_l, the dislocation can overcome the pinning and get through. It is found that σ_l reaches its maximum at a transition temperature, which is about 350 K. Also revealed in the simulations is a generalized dislocation dissociation that a 60° dislocation, while interacting with a vacancy cluster, can result in 30° and 90° partial dislocations when the applied shear stress reaches another critical value σ_h. The two resultant partial dislocations are separated by an intrinsic stacking fault. Unlike σ_l, σ_h keeps decreasing at temperatures higher than 400 K and remains a constant at lower temperatures.

DOI: 10.1103/PhysRevB.77.045211 PACS number(s): 61.72.Lk, 61.72.Qq, 71.15.Pd

I. INTRODUCTION

Dislocations, well known to be responsible for a plastic behavior in general and to act as trapping and scattering centers for electronic carriers, play a fundamental role in semiconductors both mechanically and electronically. A large number of theoretical and experimental studies on their properties have been conducted since their discovery (see, for example, Refs. 1–4). In this work, we will focus on the dislocations in silicon.

A well known type of dislocation in silicon is the 60° one, which lies on {111} slip planes and has a Burgers vector of $(a/2)\ \langle 110\rangle$, where a is the lattice parameter. Due to the nonprimitive unit cell, there are two distinct sets of {111} planes: the closely spaced glide subset and the widely spaced shuffle subset.[5] In addition, the glide dislocation will dissociate into a pair of partial dislocations separated by an intrinsic stacking fault.[6–8] Shuffle subset dislocation, on the contrary, has been less studied. Some early work about these two kinds of dislocations can be found in Justo *et al.*[9] In addition to dislocations, vacancies of high concentration are common in silicon and are usually generated during a variety of processes such as implantation, irradiation, and etching. The vacancies will interact with defects and impurities. However, the interaction between the vacancy cluster and the shuffle dislocations, although of great importance, has received less attention and still remains an open problem.

In the present work, a model consisting of a 60° shuffle dislocation dipole and a vacancy cluster subjected to an applied shear stress is first established. A series of molecular dynamics simulations is then carried out at different temperatures and external loadings to study the vacancy-dislocation interactions.

II. COMPUTATIONAL MODEL

To simplify the computational model, dislocations are introduced in the form of dipoles, giving zero net Burgers vectors and enabling as well the use of periodic boundary conditions (PBCs) in all three dimensions. Note that two types of interactions, one between the two dislocations forming the dipole and one between the dipole and its image due to the PBC, are quite weak,[10] and hence are neglected for simplicity.

For the construction of the initial vacancy configuration, Estreicher *et al.*[11] found that the lowest-energy state of all V_N's $(N=1,2,\ldots,6)$ vacancy clusters occurs when the Si atoms are removed successively from a hexagonal ring in the crystal. This indicates that V_6 is remarkably stable. As shown in Fig. 1, the configurations in which atoms marked by 1-2-3-4-5-6 or 9-10-11-12-13-14 are removed can be regarded as glide types, and the configurations 7-8-9-14-13-15, 4-7-8-9-10-11, and 4-7-15-13-12-11 are taken as shuffle I, shuffle II, and shuffle III, respectively.

In this work, the cell vectors of the supercell in three dimensions are $20[11\bar{2}]$, $14[111]$, and $6[1\bar{1}0]$ with sizes of 13.30, 13.17, and 2.31 nm, respectively. Details on the creation of the dislocation dipole can be found in our earlier work.[12] The dipoles created, marked by B and C in Fig. 2, are of 60° shuffle-set character having opposite Burgers vectors $(a/2)[10\bar{1}]$ and $(a/2)[\bar{1}01]$, respectively. Note that dislocations B and C align along $[1\bar{1}0]$ on the (111) slip plane and are separated from each other by a distance of $6a[111]$.

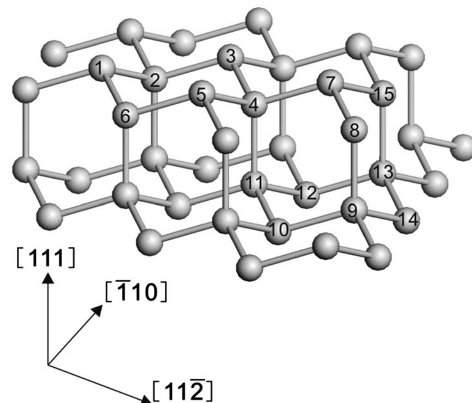

FIG. 1. Schematic diagram showing the V_6 vacancy defects.

 ©2008 The American Physical Society

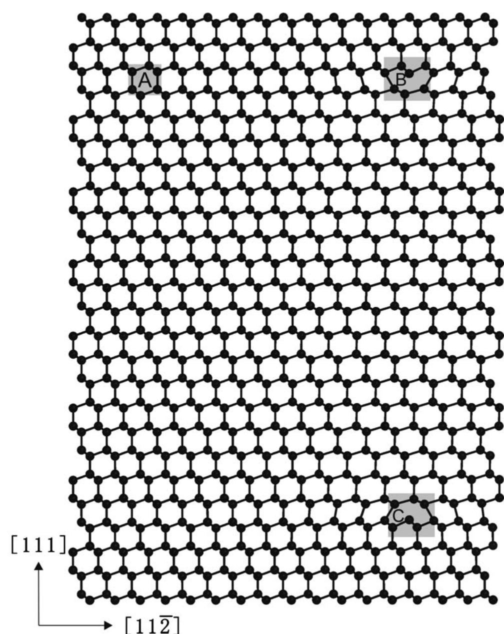

FIG. 2. Atomic configuration with the 60° dislocation dipole (marked by B and C) and the V_6 vacancy defects (marked by A).

A shuffle III V_6, marked by A in Fig. 2, is placed halfway to the front and rear surfaces of the simulation box. Note that V_6 at A also lies on the slip plane of dislocation B, and the distance between them is about $4[11\bar{2}]$. In the following sections, we will study the interaction between A and B using the molecular dynamics simulations.

III. SIMULATION METHOD

Molecular dynamics simulations are conducted under constant applied shear stress and at constant temperature. Specifically, we utilize two kinds of interatomic potentials, the Stillinger-Weber (SW) potential[13] and the environment-dependent interatomic potential (EDIP).[14] As stated previously, PBCs are adopted in all three dimensions. If not specified otherwise, the time step for all simulations is 1 fs. To achieve the constant temperature, the initial system is relaxed for 2000 steps at 0 K followed by a gradual adjusting procedure, with the temperature raised 50 K every 2000 steps until the desired temperature is obtained. After that, the system temperature is kept constant using an atom velocity rescaling algorithm.[15] Finally, the external shear stress is applied by means of the Parrinello-Rahman method.[16]

Without loss of generality, we direct the shear stress along the Burgers vector since only the stress component parallel to the Burgers vector does work. Simulations with a wide range of final system temperatures running from 100 to 900 K, subjected to an applied shear stress ranging from 100 to 3000 MPa, are conducted. The simulation results are given below.

IV. RESULTS AND DISCUSSION

Due to the Peierls barrier in silicon crystal, at low shear stress, dislocations are not able to glide.[12] When a higher stress is applied, dislocations B and C are observed to move in opposite directions on their own slip planes. Dislocation B is then expected to move closer to the V_6 located at A. The interaction between A and B can thus be studied in detail. It is found that when the dislocation reaches the site of the vacancy cluster, it gets pinned. This is for a moderate external stress. If the stress is raised gradually, there exists a critical level at which the pinned dislocation can be released. This critical stress is recorded as σ_l.

The process of the unpinning is depicted in Fig. 3. When the dislocation encounters the vacancy cluster, it stretches and then breaks into two segments, each having one end rooted on the surface of the vacancy cluster. These rooted ends are dragged by their corresponding free arms. If the applied stress is higher than σ_l, the barrier can be overcome and the two rooted ends will be pulled forwardly and will slide on the surface of the vacancy cluster. The two dislocation segments then reconnect when they get off. The variation of stress σ_l as a function of temperatures T using the SW potential is shown in the solid line in Fig. 4. It can be seen that σ_l increases as the temperature increases when $T < 350$ K, and then decreases as the temperature increases when $T > 350$ K.

The existence of the transition temperature implies that at least one of the driving and the resisting factors shows a strong temperature dependence. Based on the physical process, it is reasonable to assume that σ_l is likely to be independent of the size of the vacancy cluster. Then, the possible major factors that control the temperature dependence of stress σ_l are the impact velocity at which the dislocation hits the vacancy cluster and the kinetic process of sliding of the rooted ends on the surface of the vacancy cluster, both of which are indeed strongly temperature dependent. Based on these considerations, we propose the following model to explain the observed phenomenon. At low temperature, the impact velocity is high,[12] so it is easy for the dislocation to get through the vacancy. At high temperature, the dislocation moves slowly along the applied stress direction[12] since the high mobility due to high temperature enables a zigzag kink motion that hinders the glide motion. However, the kink motion will choose the lowest resistance path for the dislocation while its roots travel on the vacancy surface, so the dislocation can also pass through the vacancy easily. At some intermediate temperature, as expected, a higher external loading is required to overcome a higher barrier than those at low or high temperatures.

In order to verify the above model, a different interatomic potential—the EDIP potential—is adopted to repeat the process. The results are shown in Fig. 4 in the dotted line. In spite of some reasonable differences in numerical values, the trend is exactly the same. However, some detailed processes still remain open problems, thus requiring further work in the future.

If the applied shear stress is further increased to a certain level, the dislocation will not simply overcome the pinning and get through the vacancy cluster; instead, it will spawn a new dislocation dipole when it passes through. Such a stress level is recorded as σ_h, and the typical stages of formation of the new dipole are shown in Fig. 5. Similarly, the variation of σ_h versus the temperature can be determined from simula-

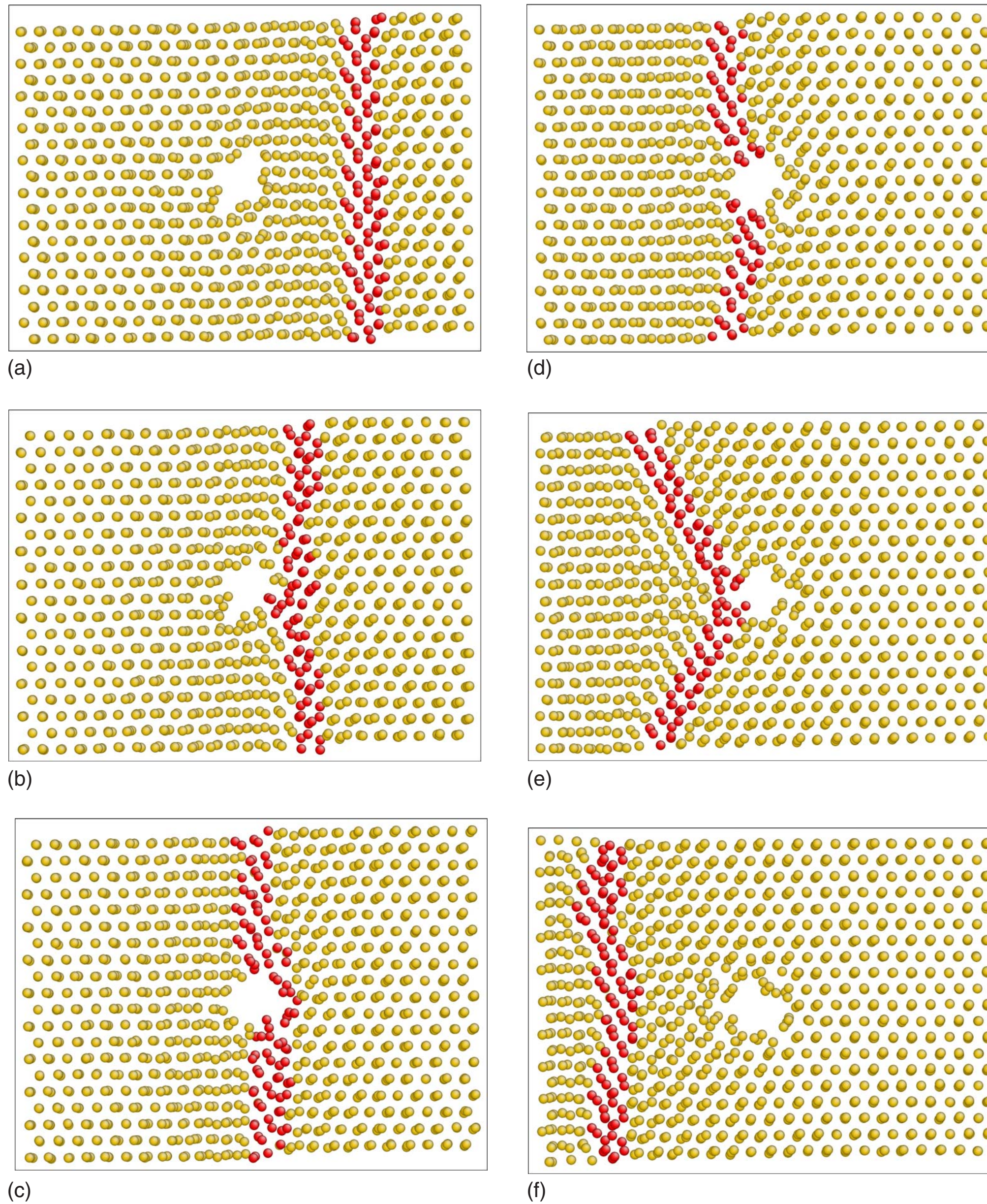

FIG. 3. (Color online) The processes of the dislocation overcoming the pinning effect.

tions and is shown in the dash-dotted line in Fig. 3. The result shows that σ_h remains a constant when the temperature is less than about 400 K and decreases as the temperature runs higher. However, note that the above observation is only valid for the SW potential. For the EDIP potential, the critical stress σ_h cannot be obtained since the EDIP potential will lead to a simulation collapse soon after the formation of the new dislocations.

The aforementioned dipole generation marks a possible mechanism of dislocation multiplication and thus deserves a detailed study. In the following text, dynamic behaviors of the dislocation and the vacancy cluster during and shortly after this process will be presented one at a time.

We first focus on the behavior of the dislocation. Figure 5(a) shows the preinteraction stage where, driven by the shear stress, the dislocation keeps moving on its slip plane and is ready to interact with the vacancy cluster. As shown in Fig. 5(b), a new dislocation dipole separated by an intrinsic stacking fault forms. The new dislocations are two 30° shuffle dislocations (vacancylike structure) with opposite Burgers vectors. Meanwhile, the 60° dislocation climbs onto another (111) slip plane below and remains on that plane afterward. The left-going 30° dislocation follows the motion of the 60° dislocation on its own slip plane. In Fig. 5(c), they begin to separate since the 60° dislocation moves faster. This 60° dislocation will reenter the simulation box on the right due to the enforced PBC, and will encounter the newly formed right-going 30° dislocation. They have opposite Burgers vectors and will thus interact. Finally, a 90° glide partial dislocation (SP structure) occurs [see Fig. 5(d)]. After that, no more glide is observed about the two remaining partial dislocations (the 30° and the 90° ones) during the later simulation. The details of their core structures are shown in Fig. 6.

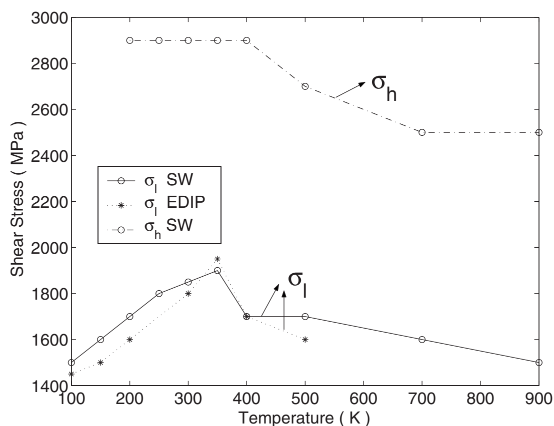

FIG. 4. The critical stress versus temperature during the interaction process. The solid line represents the critical stress (σ_l) when the dislocation is unpinned. The dotted line represents the σ_l obtained by the EDIP potential. The dash-dotted line represents the critical stress (σ_h) when the new dislocations are formed.

We then switch to the vacancy cluster. A typical evolution of the vacancy cluster during the interaction is shown in Fig. 7. It is obvious that the structure of the vacancy cluster is reconstructed during the initial stage of the interaction [Figs. 7(a)–7(c)]. During the stages that follow, the new dislocation dipole appears and the bonds are broken and reformed [Figs. 7(d)–7(h)].

Based on the above results, if the simulation system is treated as a black box, for the 60° dislocation interacting with the vacancy cluster, the following reaction occurs under the external loading σ_h:

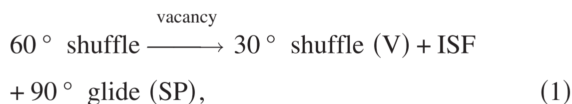

$$60^\circ \text{ shuffle} \xrightarrow{\text{vacancy}} 30^\circ \text{ shuffle (V)} + \text{ISF} + 90^\circ \text{ glide (SP)}, \quad (1)$$

where the Burgers vector remains the same before and after the reaction. Obviously, this is different with a relevant ordinary dislocation dissociation as proposed in Refs. 17 and 18

$$60^\circ \text{ shuffle} \rightarrow 30^\circ \text{ glide} + \text{ISF} + 90^\circ \text{ shuffle}, \quad (2)$$

which is on-site and energetically self-promoted. Here, however, the successive reactions occur at different locations; hence, the above proposed scheme in Eq. (1) for dislocation dissociation can only be understood in the general sense. Note further that without the vacancy cluster and applied stress, such generalized dissociation is not possible.

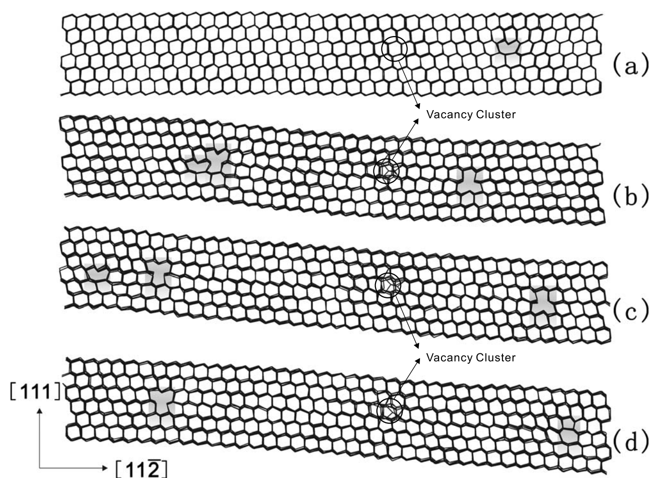

FIG. 5. The stages of formation of new dislocations during the 60° dislocation interaction with the vacancy cluster. The shaded region represents the core structures.

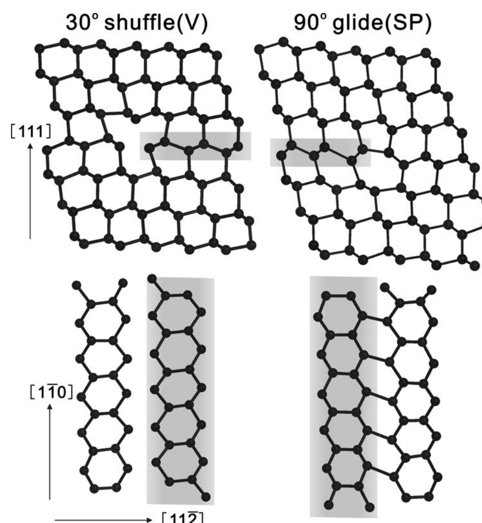

FIG. 6. The core structures of the 30° and 90° partial dislocations. The upper figure shows the view along the dislocation line, and the lower figure shows the (111) glide plane. The shaded region represents the intrinsic stacking fault. (V) is for vacancylike structure, and (SP) is for single period.

V. CONCLUSIONS

In this work, the interaction of a 60° shuffle dislocation and a vacancy cluster (V_6) in silicon are studied via the molecular dynamics method equipped with the Stillinger-Weber and EDIP potentials. The dynamic behaviors of the dislocation and vacancy cluster under varying applied stresses and

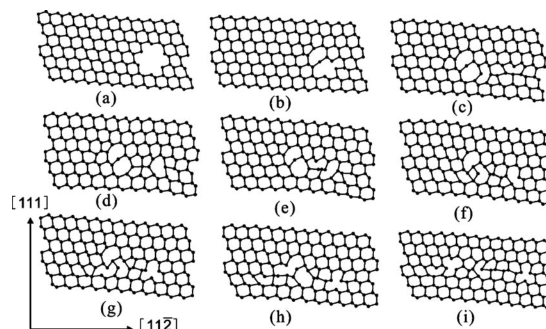

FIG. 7. Temporal cross-sectional projections of the atomic configuration of two layers containing the vacancy cluster and the 60° dislocation. [Note that the dislocation in (a) and (b) is far away from the vacancy cluster, thus not shown.]

temperatures reveal many interesting points. It is found that at relatively low stress, the dislocation gets pinned. With the load increased, there exist two critical levels at which the dislocations show distinct dynamic behaviors. At the lower critical stress level, the dislocation can be unpinned to glide on its slip plane, while at the higher one, a 30° shuffle dislocation dipole forms when the 60° shuffle dislocation passes through. Variations of the two critical stresses with temperature are also obtained. The lower critical stress is found to achieve its maximum at a temperature around 350 K, while the higher critical one remains a constant below 400 K and decreases when temperature runs above.

At the higher critical stress level, it is also found that a dislocation dissociation in the generalized sense occurs, where the 60° dislocation and the 30° dislocation that move in the opposite directions in the newly formed dislocation dipole will eventually react, and a 90° dislocation occurs. If the system is viewed as a black box, then a 60° shuffle dislocation will dissociate into one 30° and one 90° partial dislocation separated by an intrinsic stacking fault.

ACKNOWLEDGMENTS

The authors gratefully acknowledge many helpful discussions with Chong He and Yubao Zhen. The authors also acknowledge Zhen for helping with the language.

*lechexi@gmail.com

[1] P. B. Hirsch, Mater. Sci. Technol. **1**, 666 (1985).

[2] H. Alexander and H. Teichler, in *Materials Science and Technology*, edited by R. W. Cahn, P. Hassen, and E. J. Kramer (VCH Weinheim, Cambridge, 1993), Vol. 4, p. 249.

[3] V. V. Bulatov, J. F. Justo, Wei Cai, S. Yip, A. S. Argon, T. Lenosky, M. de Koning, and T. Diaz de la Rubia, Philos. Mag. A **81**, 1257 (2001).

[4] A. T. Blumenau, R. Jones, and T. Frauenheim, J. Phys.: Condens. Matter **15**, S2951 (2003).

[5] M. S. Duesbery and B. Joos, Philos. Mag. Lett. **74**, 253 (1996).

[6] R. W. Nunes, J. Bennetto, and David Vanderbilt, Phys. Rev. B **57**, 10388 (1998).

[7] J. F. Justo, V. V. Bulatov, and S. Yip, J. Appl. Phys. **86**, 4249 (1999).

[8] A. T. Blumenau, R. Jones, T. Frauenheim, B. Willems, O. I. Lebedev, G. Van Tendeloo, D. Fisher, and P. M. Martineau, Phys. Rev. B **68**, 014115 (2003).

[9] J. F. Justo, M. de Koning, Wei Cai, and V. V. Bulatov, Phys. Rev. Lett. **84**, 2172 (2000).

[10] Jinpeng Chang, Wei Cai, V. V. Bulatov, and S. Yip, Comput. Mater. Sci. **23**, 111 (2002).

[11] S. K. Estreicher, J. L. Hastings, and P. A. Fedders, Appl. Phys. Lett. **70**, 432 (1997).

[12] C. X. Li, Q. Y. Meng, G. Li, and L. J. Yang, Superlattices Microstruct. **40**, 113 (2006).

[13] F. H. Stillinger and T. A. Weber, Phys. Rev. B **31**, 5262 (1985).

[14] J. F. Justo, M. Z. Bazant, E. Kaxiras, V. V. Bulatov, and S. Yip, Phys. Rev. B **58**, 2539 (1998).

[15] H. Andersen, J. Chem. Phys. **72**, 2384 (1980).

[16] M. Parrinello and A. Rahman, Phys. Rev. Lett. **45**, 1196 (1980).

[17] A. Gomez, D. H. J. Cockayne, P. B. Hirsch, and V. Vitek, Philos. Mag. **31**, 105 (1975).

[18] A. T. Blumenau, M. I. Heggie, C. J. Fall, R. Jones, and T. Frauenheim, Phys. Rev. B **65**, 205205 (2002).